Received: 30 November 2018 | Revised: 28 May 2019 | Accepted: 31 May 2019

DOI: 10.1002/hbm.24698

RESEARCH ARTICLE

WILEY

A machine learning investigation of volumetric and functional MRI abnormalities in adults born preterm

Jing Shang[1,2] | Paul Fisher[1] | Josef G. Bäuml[2,3] | Marcel Daamen[4,5] | Nicole Baumann[6] | Claus Zimmer[3] | Peter Bartmann[4] | Henning Boecker[5] | Dieter Wolke[6,7] | Christian Sorg[2,3,8] | Nikolaos Koutsouleris[1] | Dominic B. Dwyer[1]

[1]Department of Psychiatry and Psychotherapy, Ludwig-Maximilian-University, Munich, Germany

[2]TUM-NIC Neuroimaging Center, Technische Universität München

[3]Department of Neuroradiology, Klinikum rechts der Isar and Technische Universität München, Munich, Germany

[4]Department of Neonatology, University Hospital Bonn, Bonn, Germany

[5]Functional Neuroimaging Group, Department of Radiology, University Hospital Bonn, Bonn, Germany

[6]Department of Psychology, University of Warwick, Coventry, United Kingdom

[7]Warwick Medical School, University of Warwick, Coventry, United Kingdom

[8]Department of Psychiatry, Klinikum rechts der Isar and Technische Universität München, Munich, Germany

Correspondence
Christian Sorg, Department of Psychiatry and Neuroradiology, Klinikum rechts der Isar, Ismaninger Strasse 22, 81675 Munich, Germany.
Email: christian.sorg@tum.de

Funding information
PRONIA, Grant/Award Number: 602152; Kommission für Klinische Forschung, Technische Universität München, Grant/Award Number: KKF 8765162; German Federal Ministry of Education and Science, Grant/Award Numbers: BMBF 01ER0803, BMBF 01ER0801; Deutsche Forschungsgemeinschaft, Grant/Award Number: 1336/1-1; Chinese Scholar Council, Grant/Award Number: 201708080036

Abstract

Imaging studies have characterized functional and structural brain abnormalities in adults after premature birth, but these investigations have mostly used univariate methods that do not account for hypothesized interdependencies between brain regions or quantify accuracy in identifying individuals. To overcome these limitations, we used multivariate machine learning to identify gray matter volume (GMV) and amplitude of low frequency fluctuations (ALFF) brain patterns that best classify young adults born very preterm/very low birth weight (VP/VLBW; n = 94) from those born full-term (FT; n = 92). We then compared the spatial maps of the structural and functional brain signatures and validated them by assessing associations with clinical birth history and basic cognitive variables. Premature birth could be predicted with a balanced accuracy of 80.7% using GMV and 77.4% using ALFF. GMV predictions were mediated by a pattern of subcortical and middle temporal reductions and volumetric increases of the lateral prefrontal, medial prefrontal, and superior temporal gyrus regions. ALFF predictions were characterized by a pattern including increases in the thalamus, pre- and postcentral gyri, and parietal lobes, in addition to decreases in the superior temporal gyri bilaterally. Decision scores from each classification, assessing the degree to which an individual was classified as a VP/VLBW case, were predicted by the number of days in neonatal hospitalization and birth weight. ALFF decision scores also contributed to the prediction of general IQ, which highlighted their potential clinical significance. Combined, the results clarified previous research and suggested that primary subcortical and temporal damage may be accompanied by disrupted neurodevelopment of the cortex.

KEYWORDS
ALFF, machine learning, multivariate, premature birth, resting-state fMRI, VBM

1 | INTRODUCTION

Multiple in-vivo imaging studies in humans have demonstrated widespread structural brain abnormalities after very premature birth (i.e., very preterm birth with gestational age < 32 weeks, VP, and/or birth with very low birth weight < 1,500 g, VLBW), with differences being found in newborns, children, adolescents, and adults (Ball et al., 2012; de Kieviet, Zoetebier, van Elburg, Vermeulen, & Oosterlaan, 2012; Nosarti et al., 2008). Functional brain imaging has also revealed widely distributed changes in brain activity in very premature born

individuals, which partly overlap with structural changes (Baldoli et al., 2015; Bauml et al., 2014; Froudist-Walsh et al., 2015; Meng et al., 2015). These abnormalities have been linked to pathophysiological cascades that begin at birth and radiate from subcortical injuries, such as hypoxic–ischemic damage to the periventricular white matter (de Vries, Benders, & Groenendaal, 2015; Thompson et al., 2014; Tsimis et al., 2015).

Until recently, research has predominantly used mass-univariate testing to make downstream inferences regarding pathological signatures of preterm birth in adolescents and adults. For example, a common hypothesis is that periventricular white matter injury impacts the development of premyelinating oligodendrocytes and subplate neurons resulting in an impaired development of thalamo-cortical connectivity (Grothe et al., 2017; Hoerder-Suabedissen & Molnar, 2015; Thompson et al., 2014), which then leads to the reduced thalamus gray matter volume (GMV) and related widely distributed white matter changes seen in adulthood (Meng et al., 2015; Joseph J. Volpe, 2009). Structural damage and downstream abnormalities are also thought to be linked to functional changes, as evident in univariate task-based and resting-state MRI studies (Baldoli et al., 2015; Bauml et al., 2014; Froudist-Walsh et al., 2015; Meng et al., 2015; Shang et al., 2018).

A straightforward technique to measure brain functioning is the amplitude of low-frequency fluctuations (ALFF) (Zang et al., 2007). Low frequency fluctuations of the blood-oxygenation level-dependent fMRI signal putatively arise from the spontaneous neural activity of microcircuits and reflect the functional integrity of the brain (Sanchez-Vives, Massimini, & Mattia, 2017). These fluctuations are sensitive to changes in brain development (Smyser et al., 2013; Wu et al., 2016), aging (Biswal et al., 2010), cognitive deficits (Z. Deng, Chandrasekaran, Wang, & Wong, 2016; Takeuchi et al., 2015), psychiatric illness (Hare et al., 2016; Lui et al., 2015; Meda et al., 2015; Zhao et al., 2017), and neurodevelopmental disorders (Itahashi et al., 2015; F. Li et al., 2014; R. Li et al., 2015; Mascali et al., 2015). Previous research in newborns born prematurely has found reduced ALFF in the bilateral superior temporal gyri and increased ALFF of the precuneus and inferior temporal gyrus (Wu et al., 2016), but ALFF research in adults born preterm is limited (Shang et al., 2018).

Both structural imaging and ALFF studies are also limited because they do not explicitly model interdependencies that would be expected given the hypothesis of a neurodevelopmental pathophysiological cascade, except for some notable exceptions. Specifically, anatomical covariance analysis in adults born preterm indicates two primary signatures: (a) a pattern of brain volume reductions across subcortical and medial temporal regions thought to be related to early brain damage; and (b) a pattern of increased frontal and lateral temporo-parietal cortical volume hypothesized to be related to disruptions in neurodevelopment (Karolis et al., 2017; Nosarti et al., 2011; Scheinost et al., 2015). However, this multivariate research has not been conducted within pipelines designed to assess generalizability, determined whether such patterns are sensitive and specific enough to identify individuals, determined how structural and functional patterns intersect, or validated them by demonstrating associations between brain maps, medical history, and cognitive performance. The potential clinical utility of such patterns in terms of their ability to predict cognitive domains that normally require laborious assessments has also not been investigated.

In order to address previous limitations, in this study we aimed to use multivariate machine learning methods to classify young adults born prematurely when compared to those full-term born on the basis of volumetric and ALFF brain abnormalities within a repeated, nested cross-validation design. We then compared the structural and functional preterm signatures, validated them by assessing their relationship to birth history and cognitive performance, and determined the potential clinical utility of the signatures by assessing their unique contribution to the prediction of the intelligence quotient. We expected to find a volumetric map containing subcortical decreases and cortical increases (Karolis et al., 2017); this signature was hypothesized to spatially overlap with the functional abnormality signature, and the degree to which the individuals loaded on the signatures was expected to correlate with the degree to which they were born prematurely (i.e., earlier birth, higher loading on the map). We also expected that the brain signatures would increase the accuracy of predicting the intelligence quotient over-and-above clinical prematurity data alone due to the close links between intelligence and functional brain networks (Dubois, Galdi, Paul, & Adolphs, 2018).

2 | MATERIALS AND METHODS

2.1 | Participants

Participants were recruited as part of the prospective Bavarian Longitudinal Study (BLS) (Riegel, Orth, Wolke, & Osterlund, 1995; Wolke & Meyer, 1999), a geographically defined whole-population study of neonatal at-risk infants born in South Bavaria. Of the initial 682 infants born VP/VLBW, 411 were eligible for the 26-year follow-up assessment, and 260 (63.3%) participated in psychological assessments (Breeman, Jaekel, Baumann, Bartmann, & Wolke, 2015). Of the initial 916 term born control infants from the same obstetric hospitals and alive at 6 years, 350 were randomly selected as term controls within the stratification variables of sex and family socioeconomic status in order to be comparable with the VP/VLBW sample. Of these, 308 were eligible for the 26-year follow-up assessment, and 229 (74.4%) participated in psychological assessments. Of the sample assessed in adulthood, 101 VP/VLBW as well as 102 FT individuals underwent MRI at 26 years of age. MRI assessments were carried out at two different sites: the Department of Neuroradiology, Klinikum rechts der Isar, Technische Universität München, Germany (N = 138), and the Department of Radiology, University Hospital Bonn, Germany (N = 67). Previous research using subsets of this sample has been published (Bauml et al., 2014; Daamen et al., 2014; Daamen et al., 2015; Grothe et al., 2017; Jurcoane et al., 2015; Meng et al., 2015; Shang et al., 2018). The study was approved by the local ethics committees of the Klinikum rechts der Isar and University Hospital Bonn. All study participants gave written informed consent and received travel expenses and a payment for attendance. A detailed description of participants, particularly including MRI-based brain abnormalities, can be found in Data S1.

2.2 | Birth-related variables

Gestational age (GA) was estimated from maternal reports of the last menstrual period and serial ultrasounds during pregnancy. In cases where the two measures differed by more than 2 weeks, clinical assessment with the Dubowitz method was applied (Dubowitz, Dubowitz, & Goldberg, 1970). Birth weight (BW), Intensity of Neonatal Treatment Index (INTI), duration of Neonatal Treatment Index (DNTI), optimality score of neonatal conditions (OPTN), days in hospital, maternal age, and familiar socioeconomic status (SES) at birth, were obtained from neonatal and obstetric records (Gutbrod, Wolke, Soehne, Ohrt, & Riegel, 2000; Riegel et al., 1995).

2.3 | Cognitive assessments

Adult general cognitive performance was assessed by independent, trained psychologists with the German version of the Wechsler Adult Intelligence Scale (WAIS III) (von Aster, Neubauer, & Horn, 2006) and converted to age-normed verbal intelligence quotient (IQ), performance IQ, and Full-Scale IQ scores at the average age of 26 years.

2.4 | Image acquisition

At both sites, MRI data acquisition was initially performed on Philips Achieva 3 T TX systems (Achieva, Philips), using an 8-channel SENSE head coil. Due to a scanner upgrade, data acquisition in Munich and Bonn had to switch to Philips Ingenia 3 T system with an 8-channel SENSE head coil, respectively, for Munich after $N = 133$ participants and for Bonn after $N = 17$ participants. To account for possible confounds introduced by scanner differences, data analyses included scanner identities as covariates of no interest. Across all scanners, sequence parameters were kept identical. Scanners were checked regularly to provide optimal scanning conditions. MRI physicists at the Klinikum rechts der Isar Munich and University Hospital Bonn regularly scanned imaging phantoms, to ensure within-scanner signal stability over time. Signal-to-noise ratio (SNR) was not significantly different between scanners (one-way ANOVA with factor "scanner-ID" [Bonn 1, Bonn 2, Munich 1, Munich 2]; $F(3,182) = 1.84$, $p = .11$). Rs-fMRI data were collected for 10 min 52 s from a gradient-echo echo-planar sequence (TE = 35 ms, TR = 2,608 ms, flip angle = 90°, FOV = 230 mm^2, matrix size = 64 × 63, 41 slices, thickness 3.58 and 0 mm interslice gap, reconstructed voxel size = 3.59 × 3.59 × 3.59 mm^3) resulting in 250 volumes of rs-fMRI data per subject. Subsequently, a high-resolution T1-weighted 3D-MPRAGE sequence (TI = 1,300 ms, TR = 7.7 ms, TE = 3.9 ms, flip angle = 15°; 180 sagittal slices, FOV = 256 × 256 × 180 mm, reconstruction matrix = 256 × 256; reconstructed voxel size = 1 × 1 × 1 mm^3) was acquired. Immediately before undergoing the resting-state sequence, subjects were instructed to keep their eyes closed and to restrain from falling asleep. We verified that subjects stayed awake by interrogating via intercom immediately after the rs-fMRI scan.

2.5 | MRI data analysis—preprocessing, outcome measures, and control for confounding effects

2.5.1 | Structural MRI data analysis—preprocessing and gray matter volume

For sMRI data analysis, we used the CAT12 toolbox (Structural Brain Mapping group, Jena University Hospital, Jena, Germany) implemented in SPM12 (Statistical Parametric Mapping, Institute of Neurology, London, UK). T1-weighted images were corrected for bias-field inhomogeneity, registered using linear (12-parameter affine) and nonlinear transformations, then spatially normalized using the DARTEL algorithm to the MNI atlas (Ashburner, 2007) and segmented into gray matter, white matter, and cerebrospinal fluid (Ashburner & Friston, 2005). The modulated normalized GMV were used in further analyses. After preprocessing all scans passed through a CAT12 automated quality check protocol. We also calculated total intracranial volume (TIV) for each subject, which was used as a covariate in further analyses.

2.5.2 | Resting-state fMRI data analysis (ALFF)

Preprocessing and measure definition were carried out using SPM12 (http://www.fil.ion.ucl.ac.uk/spm) and DPARSF (Chao-Gan & Yu-Feng, 2010). For each participant, functional volumes were realigned to correct for head motion and coregistered to each subject's high-resolution structural T1 image. To transform individual images into common MNI (Montreal Neurological Institute) space, segmentation-based normalization parameters were applied to the coregistered structural and functional data. Data from 17 subjects (7 VP/VLBW subjects and 10 FT subjects) were excluded from further analysis due to excessive head motion defined as a cumulative translation or rotation >3 mm or 3°. To estimate motion-induced artifacts, temporal SNR (tSNR), point-to-point head motion, and frame-wise displacement were assessed for each subject (Murphy, Bodurka, & Bandettini, 2007; Power, Barnes, Snyder, Schlaggar, & Petersen, 2012; Van Dijk, Sabuncu, & Buckner, 2012). Two-sample t tests yielded no significant differences between groups regarding mean point-to-point translation or rotation of any direction ($p > .1$), tSNR ($p > .25$), and frame-wise displacement ($p > .3$). We did not apply additional "scrubbing" procedures to remove outliers in rs-fMRI volumes (Power et al., 2012), following the suggestions of Babu and Stoica (2010) and Yan et al. (2013)). In particular, removal of noncontiguous time points alters the underlying temporal structure of the data, which precludes conventional frequency-based analyses of rs-fMRI data (i.e., the fast Fourier transformation-based ALFF).

To determine ALFF, nuisance covariates, including six head motion parameters, white matter, and cerebrospinal fluid signal intensities were regressed out from preprocessed rs-fMRI data. Then, after linear-trend removal, the time series were transformed to the frequency domain using Fast Fourier Transformation to obtain the power spectrum. ALFF was calculated by taking the square root of the power spectrum averaged across 0.01–0.1 Hz at each voxel. Finally, the ALFF was standardized by dividing each voxel's value by the global mean (Zang et al., 2007).

2.6 | Multivariate pattern classification analysis for GMV and ALFF

We used the NeuroMiner pattern recognition tool (www.pronia.eu/neurominer) to implement two fully automated machine learning pipelines to characterize multivariate brain patterns that separated full-term born control subjects from VP/VLBW individuals using, respectively: (a) the normalized and modulated GMV maps; and (b) the normalized ALFF maps. Models were trained within a repeated, nested cross-validation framework. In the inner loop of the cross-validation (CV), the training data were separated into 10 folds and preprocessed by: (a) smoothing the images with a full-width by half maximum smoothing kernel across range of 4, 6, 8, 10 mm; (b) correction for age, sex, sites, and TIV; 3) dimensionality reduction using principal components analysis retaining the components contributing to the top 80% of the variance; 4) scaling [0,1]. Each processed training sample entered a stepwise forward variable selection process using a linear support vector machine (SVM; LIBSVM 3.12; http://www.csie.ntu.edu.tw/~cjlin/libsvm) at each selection step to iteratively grow a predictive group of variables up to 80% of the variable set (10% of variables added at each step). The procedure was repeated for each smoothing value and across a range of SVM C hyperparameters [0.125 0.25 0.5 1 2 4] and models that maximized the balanced accuracy (average of sensitivity and specificity) were selected within the inner CV loop. Inner folds were retrained using the winning model and the resulting inner models were applied to the outer-loop validation data. As the outer CV folds were permuted 5 times, this procedure produced an ensemble of 50 decision scores reflecting the degree to which an individual was classified as a FT or VP/VLBW. The predicted class of the individual was defined using majority voting across models in which a given participant was not involved as a training instance.

Multivariate brain patterns characterizing the decision boundary that separated FT and VP/VLBW subjects were visualized by back-projecting the feature weight vector of each SVM model from PCA to MNI space. Specifically, to visualize the average decision function, we implemented the procedure described in Koutsouleris et al. (Koutsouleris et al., 2015), involving: (a) In PCA space, the weight vector (w) of each SVM model was projected back to voxel space. This computation was performed for every training sample on the inner cross-validation (CV_1) cycle, resulting in 10 voxel-level images for a given training partition on the outer (CV_2) loop. (b) The average and standard error volumes of these 10 voxel-level w images were computed. (c) For each CV_2 partition, voxels with an absolute value greater than their respective standard error multiplied by 1.96 were set to one, or to zero otherwise. This thresholding procedure extracted only those voxels that reliably contributed to the average neuroanatomical decision boundary of a given CV_2 partition at the 95% confidence interval. (d) The obtained binary images were summed across all CV_2 partitions and divided by the number of partitions, thus forming a single map that specified every voxel's probability of reliably contributing to the average neuroanatomical decision boundary across the entire experiment.

Because we were specifically interested in the quantitative relationship between mutual structural and functional differences, we calculated the spatial overlap of both patterns according to the following steps: First, any significant clusters resulting from the SVM analysis of two modalities were saved as images in SPM12 and subsequently binarized between −1~ − 0.5 or 0.5~1. Second, clusters showing spatial overlap in both entities were resampled to common space/dimension and multiplied with each other via ImCalc to identify voxels that showed significant group differences in either domain. Resulting clusters only contained voxels that showed significant differences in both structural and functional voxel probability maps.

2.7 | Association of clinical and cognitive variables with brain signatures

We conducted two analyses in order to: (a) validate the neuroanatomical signatures by providing evidence of associations with demographics, medical history of preterm birth, and cognition; (b) determine whether the neuroanatomical signatures could enhance the prediction of intelligence over-and-above the contribution of clinical indicators of prematurity. For both analyses, decision scores separating the VP/VLBW individuals from the controls were used to quantify the degree to which each preterm individual's brain matched the VBM and ALFF maps, respectively. We first assessed univariate relationships using Spearman's correlation and then used a machine learning approach to quantify multivariate relationships. Specifically, support vector regression (nu-SVR; LIBSVM 3.12; http://www.csie.ntu.edu.tw/~cjlin/libsvm) was employed using a similar procedure as for the imaging analyses. A repeated, nested framework (10x10 in CV1, 10x10 in CV2) was employed. For each training fold, preprocessing involved: (a) scaling to a range of [0, 1]; (b) pruning noninformative columns with zero variance; (c) k-Nearest Neighbor-(k-NN) imputation to fill the missing values in the data (Jonsson & Wohlin, 2004). Each processed training sample entered a stepwise forward variable selection process using SVR at each selection step to iteratively grow a predictive group of variables up to 80% of the variable set (10% of variables added at each step). This stepwise procedure identifies the most parsimonious subset of variables within the variable pool. C parameters were optimized within the range of [0.016 0.063 0.25 1] and the nu parameter characterizing the model fit of the regression across the range of [0.2 0.5 0.7]. Inner folds were retrained using the winning model and the resulting inner models were applied to the outer-loop validation data. To investigate the contribution of individual variables we plotted the percentage of times that each feature was selected by the wrapper.

3 | RESULTS

3.1 | Sample characteristics

Group clinical-performance characteristics are shown in Table 1. The VP/VLBW and FT group did not differ with respect to age at assessment (p = .277), gender (p = .786), SES at birth (p = .253), and maternal age (p = .956). By design VP/VLBW adults had significantly lower GA (p < .001) and BW (p < .001). VP/VLBW persons had significantly more neonatal medical complications (optimality score) (p < 0.001)

TABLE 1 Clinical performance characteristics

Clinical-performance variables	Full-term group (n = 92)			VP/VLBW group (n = 94)			Statistical comparison
	M	SD	Range	M	SD	Range	
Sex (m/f)	53/39			56/38			p = .786
Age (years)	26.8	±0.7	26–29	26.7	±0.6	26–28	p = .277
GA (weeks)	39.7	±1.1	37–42	30.5	±2.0	25–36	p < .001
BW (g)	3,413	±433	2,450–4,670	1,319	±309	630–2070	p < .001
OPTI	0.4	±0.6	0–2	8.9	±2.4	3–14	p < .001
Hospital (days)	6.8	±2.4	2–15	72.8	±26.0	24–170	p < .001
DNTI				53.9	29.3	8–149	—
INTI	—	—	—	11.7	3.8	3–19.8	—
TIV	1,578.4	160.2	1,204.6–1982.9	1,507.2	143.9	1,236.2–1860.6	p = .002
SES[a]	29/41/22		1-3	27/42/25		1–3	p = .253
Maternal age (years)	29.4	±5.2	18–42	29.4	±4.7	17–41	p = .956
Full-scale IQ[b]	102.9	±11.9	77-130	94.5	±12.9	64–131	p < .001
Verbal IQ[b]	106.5	±14.3	77-143	90.4	±14.0	62–137	p = .001
Performance IQ[b]	98.5	±10.4	69-125	89.7	±13.8	56–118	p < .001

Notes: Statistical comparisons: sex, SES with χ^2 statistics; age, GA, BW, Hospital, maternal age, IQ measures, TIV with two sample t-tests; OPTI with nonparametric Mann–Whitney U-tests. OPTI, DINTI, INTI, TIV, Full-scale IQ, Verbal IQ, Performance IQ: arbitrary units.
Abbreviations: BW, birth weight; DNTI: duration of neonatal treatment index; GA, gestation age; Hospital, duration of hospitalization; INTI, intensity of neonatal treatment (morbidity) index; IQ, intelligence quotient; OPTI (neonatal), optimality score of neonatal conditions index; SES, socioeconomic status at birth; maternal age, maternal age at birth; TIV, total intracranial volume.
[a]1 = upper class, 2 = middle class, 3 = lower class.
[b]Data are based on 90 VLBW preterm and 89 full-term subjects, respectively.

and were hospitalized longer (p < .001). In addition, they had significantly lower Full-Scale IQ (p = .001), verbal IQ (p = .001), and performance IQ scores (p < .001).

3.2 | Patterns of aberrant GMV in VP/VLBW born adults

Multivariate pattern classification via SVM based on individual GMV maps separated VP/VLBW and FT participants with balanced accuracy of 80.72% (specificity 88.0%, sensitivity 73.4%, Area Under the Curve: 0.90) (Table 2). Distinguishing patterns of increased and decreased GMV, respectively, which visualize this group separation, indicate multivariate patterns of interrelated volume decreases and increases in VP/VLBW adults (Figure 1). Patterns of decreased GMV in the VP/VLBW group compared with the term controls were in the bilateral middle temporal gyri, thalamus, caudate, and hippocampus. Patterns of increased GMV were in the bilateral superior temporal gyri, medial and lateral prefrontal cortex, precuneus/posterior cingulate cortex, and occipital regions.

TABLE 2 Classification performance of very preterm/very low birth weight (VP/VLBW) based on GMV and ALFF, respectively

Binary classifiers	GMV	ALFF
TP	69	68
TN	81	76
FP	11	16
FN	25	26
Accuracy	80.7	77.4
Sensitivity, %	73.4	72.3
Specificity, %	88.0	82.6
BAC	80.7	77.5
AUC	0.90	0.85
PPV	86.3	82.0
NPV	76.4	74.5

Abbreviations: ALFF, amplitude of low-frequency fluctuations; AUC, area under the curve; BAC, balanced accuracy; GMV, gray matter volume; FN, false-negative; FP, false-positive; NPV, negative predictive value; PPV, positive predictive value; TN, true-negative; TP, true-positive.

3.3 | Patterns of aberrant ALFF in VP/VLBW adults

Multivariate pattern classification based on individual ALFF maps separated VP/VLBW and FT participants with balanced accuracy of 77.5% (specificity 82.6, sensitivity 72.3%, Area Under the Curve: 0.85) (Table 2). Patterns of decreased ALFF in the VP/VLBW group compared with the term controls were in the temporal pole, superior temporal gyrus, and inferior frontal gyrus (Figure 2). Patterns of increased ALFF were in the thalamus and the superior parietal lobes extending to the premotor cortices (Figure 2).

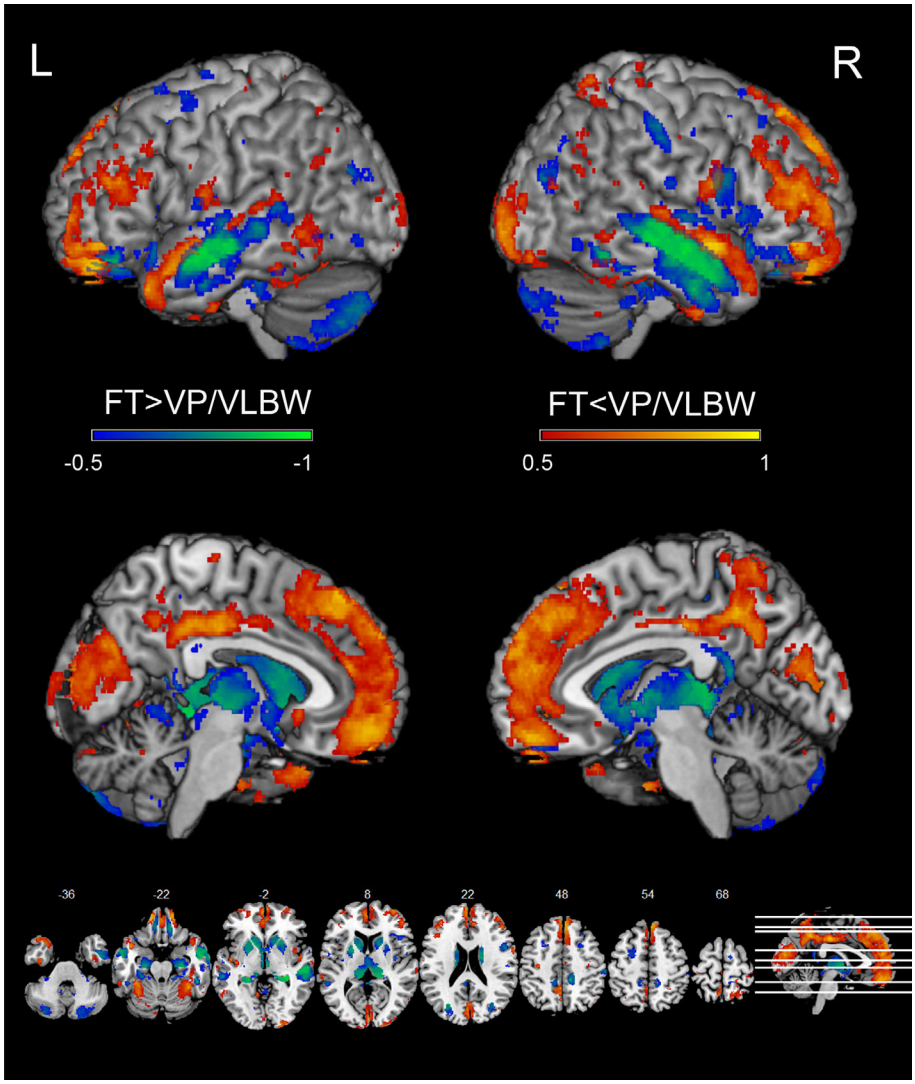

FIGURE 1 Voxel probability map of reliable contributions to the FT (full-term born) versus VP/VLBW (very preterm/very low birth weight born) group decision boundary using gray matter volume (GMV) of structural MRI data. Voxels with a probability of >50% were overlaid on the single subject MNI template using the MRIcron software package (http://www.mccauslandcenter.sc.edu/mricro/mricron/) [Color figure can be viewed at wileyonlinelibrary.com]

3.4 | Comparison of GMV and ALFF maps

The GMV and ALFF maps were largely nonoverlapping (Figures S1 and S2): First, the GMV changes were associated with subcortical decreases and frontal, medial frontal, and PCC increases; second, the ALFF maps were largely associated with decreases in the superior temporal gyri and increases in the parietal and sensorimotor cortices. Of the overlapping regions, decreases were found across both modalities in the middle temporal gyrus and right insula (Figure 3; blue). Increases were found for both modalities for the right fusiform gyrus and parietal lobes (Figure 3; red). Opposite effects were also found in the superior temporal gyrus with increased GMV but decreased ALFF (Figure 3; yellow), and decreased GMV but increased ALFF was found for the thalamus and caudate nucleus (Figure 3; violet).

3.5 | Clinical and cognitive validation

Clinical and cognitive scores predicted GMV- and ALFF-based classification decision scores, respectively (GMV: R^2 = .31, p < .001, mean average error = 0.6; ALFF: R^2 = .14, p < .001, mean average error = 0.43) (Table 3). Across both imaging modalities, increased number of hospital days and lower BW was associated with increased VP/VLBW likeness (Figure 4). For ALFF specifically a lower performance IQ and for GMV a higher total intracranial volume were associated with increased VP/VLBW likeness. Univariate correlations supported these findings as demonstrated by significant associations between GMV decision scores and BW, hospital days, GA, and the INTI (Table 4). ALFF decision scores were significantly associated with BW, GA, hospital days, the INTI, and IQ (Table 4). Full-scale IQ was predicted using a combination of clinical variables and neuroimaging decision scores (R^2 = .15, p < .001, mean average error = 9) at higher accuracies than using clinical variables alone (Table S1). Variable importance analysis showed that decision scores of ALFF and birth-related variables (e.g., hospital days and birth weight) contributed most (Figure S2). We additionally predicted general IQ using a step-wise multiple linear regression approach in order to determine the additive effects of the neuroimaging decision scores. These analyses aligned with the machine learning results to demonstrate that the prediction of full-scale IQ significantly improved after the addition of neuroimaging decision scores (clinical R^2 = .32, p = .001; clinical and imaging R^2 = 0.36, p < .001) as mediated by ALFF but not GMV (Table S2).

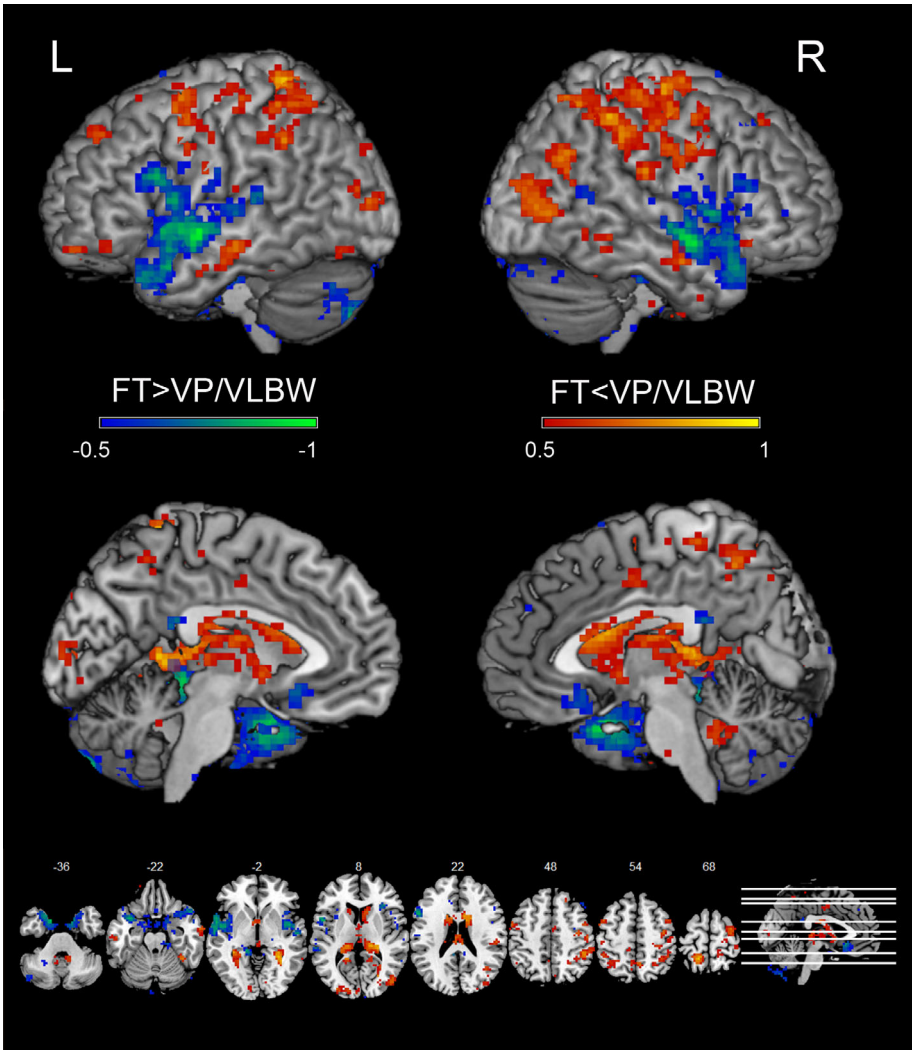

FIGURE 2 Voxel probability map of reliable contributions to the FT (full-term born) versus VP/VLBW (very preterm/very low birth weight born) group decision boundary using amplitude of low-frequency fluctuations (ALFF) of resting-state fMRI data. Voxels with a probability of >50% were overlaid on the single subject MNI template using the MRIcron software package (http://www.mccauslandcenter.sc.edu/mricro/mricron/) [Color figure can be viewed at wileyonlinelibrary.com]

4 | DISCUSSION

We analyzed structural and resting-state functional MRI data using machine learning to find that preterm birth signatures of brain abnormalities that could accurately identify individuals at a single-subject level. Our hypothesis was partially supported by the finding that subcortical volume decreases and cortical increases comprised the preterm birth signature. However, contrary to our hypothesis, the ALFF pattern was not completely overlapping and showed distinctive parietal, sensorimotor, and superior temporal cortex regions. Intersections of the maps were found in specific regions of the thalamus, insula, middle temporal cortex, and fusiform gyrus. The maps were validated by their association with critical preterm birth variables in agreement with our hypotheses and ALFF was found to contribute to the prediction of general intelligence.

4.1 | Patterns of aberrant gray matter volume

Individuals born preterm could be separated from full-term individuals on the basis of brain volume at an accuracy of 80%. The spatial brain patterns broadly agreed with previous literature (Ball et al., 2012; Karolis et al., 2017; Loh et al., 2017; Nosarti et al., 2008), but extended this research within a multivariate framework to demonstrate clearly differentiable networks of decreased and increased GMV. Decreased GMV was found in a pattern that centered on subcortical structures (thalamus, caudate, and hippocampus) and included the middle temporal gyri. Increased GMV was found in cortical structures that prominently involved the medial prefrontal cortex, dorsolateral prefrontal cortex, superior temporal gyrus, precuneus/posterior cingulate cortex, and occipital regions.

The differentiation between subcortical-temporal decreases and cortical increases could be interpreted as an interaction between primary brain pathology and secondary neurodevelopmental disruption (Joseph J. Volpe, 2009). In particular, *subcortical* brain lesions are indicated in postmortem preterm studies demonstrating neuronal loss and gliosis of the thalamus and basal ganglia (Haynes, Sleeper, Volpe, & Kinney, 2013; J. J. Volpe, 2012). This damage is indicated by reduced MRI volumes in infancy (Boardman et al., 2006; Haynes et al., 2013), which is sustained during childhood, adolescence, and adulthood (Bjuland, Rimol, Lohaugen, & Skranes, 2014; Counsell et al., 2007; Lax et al., 2013; Nosarti et al., 2008; Peterson et al., 2000; Young et al.,

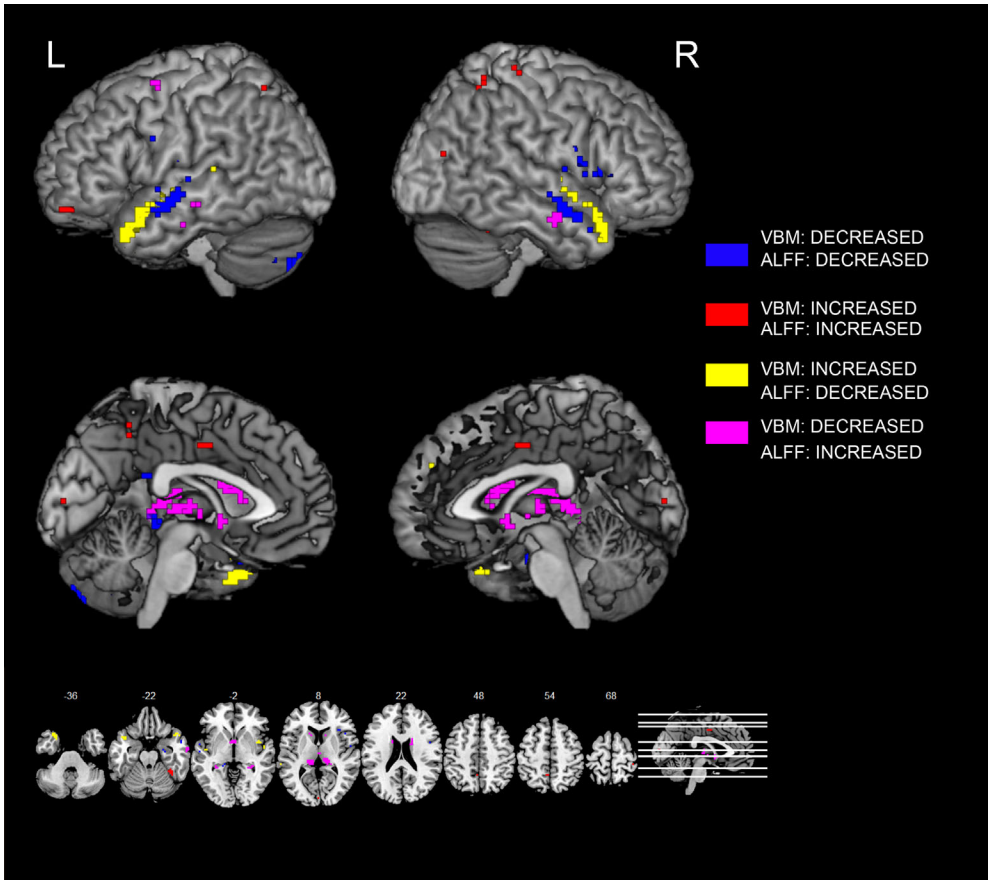

FIGURE 3 Voxel probability map of reliable contributions to the FT (full-term born) versus VP/VLBW (very preterm/ very low birth weight born) group decision boundary using decreased amplitude of low frequency fluctuations (ALFF) of resting-state fMRI data and VBM. Blue represents decreased VBM and ALFF in both middle temporal gyrus and right insular. Red represents increased VBM and ALFF in right fusiform gyrus and parietal lobes. Yellow represents areas with increased VBM but decreased in ALFF and both superior temporal gyrus and temporal lobes. Violet represents areas with decreased VBM but increased ALFF in subcortex, including the thalamus and caudate nucleus. Voxels with a probability of >50% were overlaid on the single subject MNI template using the MRIcron software package (http://www.mccauslandcenter.sc.edu/mricro/mricron/) [Color figure can be viewed at wileyonlinelibrary.com]

TABLE 3 Multiple clinical-performance scores predict decision scores for very preterm/very low birth weight (VP/VLBW) based on GMV and ALFF, respectively

nu-SVR	GMV	ALFF
COD (R^2)	30.94	13.96
Pearson r	.56	.37
P(t) value	<.001(6.42)	<.001(3.86)
MAE	0.6	0.43
MSE	0.5	0.4

Note: Multiple clinical-performance variables and support vector regression (nu-SVR) was used to predict the decision scores in 94 VP/VLBW subjects based on gray matter volume (GMV) and amplitude of low frequency fluctuation (ALFF), respectively, of Table 2 and Figures 1 and 2. Clinical-performance variables were: gender, GA, BW, OPTI (neonatal), Hospital, DNTI, INTI, SES, maternal age, adult age, intelligence quotient (including verbal, performance, and full-scale IQ) for both ALFF and GMV. TIV is only included in GMV group.
Abbreviations: ALFF, amplitude of low-frequency fluctuations; BW, birth weight; COD, coefficient of determination; DNTI, duration of neonatal treatment index; GA, gestational age, GMV, gray matter volume; INTI, intensity of neonatal treatment index; IQ, intelligence quotient; MAE, mean absolute error; MSE, mean squared error; OPTI, optimality score of birth; SES, socio-economic score; TIV total intracranial volume.

2015). In contrast, postmortem *cortical* damage is only reported in cases of severe forms of periventricular leukomylacia (Haynes et al., 2013), suggesting that localized abnormalities of cortical volume reported in preterm children or adults (Lean, Melzer, Bora, Watts, & Woodward, 2017; Nosarti et al., 2014; Wan, Wood, Chen, Wilson, & Reutens, 2013) are attributable to secondary pathological cascades that disrupt normal neurodevelopment (e.g., from thalamic, white matter, or GABAergic cellular damage) (Joseph J. Volpe, 2009).

In this study, secondary pathological cascades putatively resulted in the developmental delay or impairment of the normative process of synaptic pruning (Sowell, Thompson, Holmes, Jernigan, & Toga, 1999) within regions that are known for their relatively late maturation (Fair et al., 2008). Supportive evidence for this hypothesis can be found in previous preterm research showing increased gray matter volume in the medial frontal and cingulate regions in children (Lean et al., 2017; Nosarti et al., 2011), adolescents (Nosarti et al., 2011), and adults (Nosarti et al., 2014). As hypothesized by previous research, the specific mechanism may be related to abnormalities of the corpus callosum and long-range white matter tracts of functional networks, such as the default mode network whose main hubs were found here (i.e., medial frontal and posterior cingulate cortex) (Cui et al., 2017; Cunningham, Tomasi, & Volkow, 2017; Daamen et al., 2014; Degnan et al., 2015). As such, this study clarifies research with disparate evidence of decreases and increases of cortical volume (Lean et al., 2017; Nosarti et al., 2014; Wan et al., 2013) by showing clearly differentiated networks. The work here also extends existing research by suggesting that such abnormalities are unique to brain volume because we did not

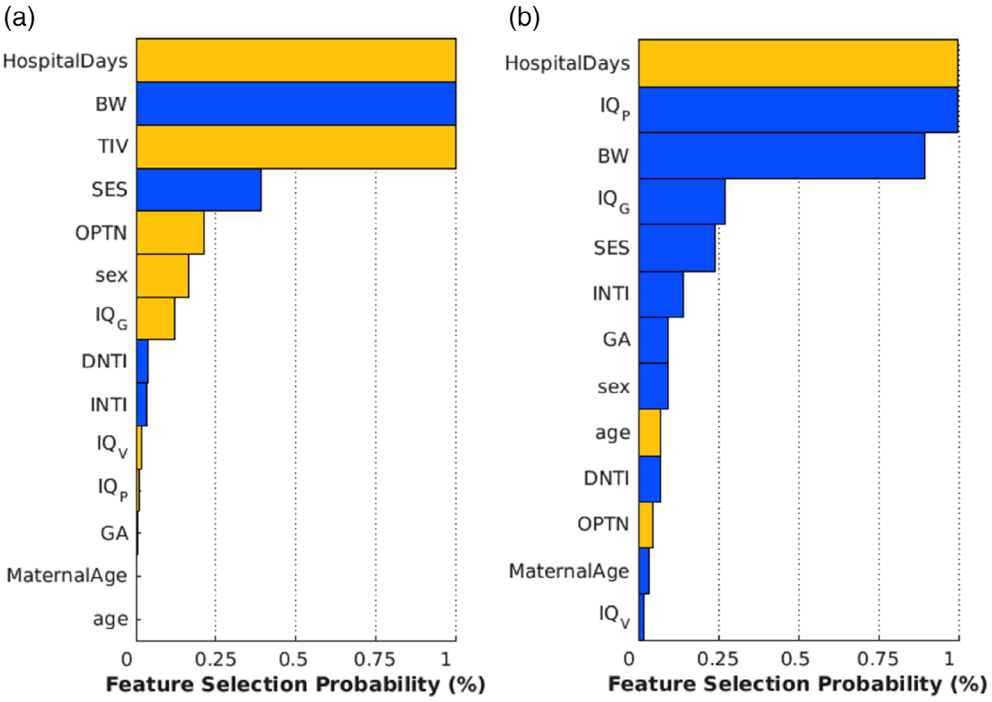

FIGURE 4 Feature selection probability showing the most reliable clinical-performance contributions to the prediction of VP/VLBW decision scores from the GMV (left) and ALFF (right) brain analyses. Yellow bars indicate positive coefficients (i.e., higher values associated with higher VP/VLBW likeness) and blue bars indicate negative weights (i.e., lower values associated with higher VP/VLBW likeness). Features above a 50% selection threshold most reliably contribute to the models. Abbreviations: BW, birth weight; DNTI, duration of neonatal treatment index; GA, gestational age; INTI, intensity of neonatal treatment index; IQG, full scale intelligence quotient; IQp, performance intelligence quotient; IQv, verbal intelligence quotient; OPTN, optimality score of neonatal treatment; TIV, total intracranial volume [Color figure can be viewed at wileyonlinelibrary.com]

find overlapping abnormal patterns of ALFF in the same medial and frontal regions.

4.2 | Patterns of aberrant ongoing brain activity fluctuations

Adults born preterm could be classified on the basis of ALFF at an accuracy of 77.5% with a pattern consisting of prominently decreased ALFF in the superior temporal cortices and temporal poles, together with increased fluctuation amplitude in thalamic, and pre- and post-central gyri. Resting-state patterns were largely nonoverlapping with volumetric patterns, except for the thalamus and middle temporal gyrus (see later). These results could be understood with reference to similar hypotheses as for brain volume regarding early primary deficit and secondary deficits.

Voxel-wise univariate research in newborn infants demonstrates reduced ALFF compared to term infants in a pattern consisting of the superior temporal gyri bilaterally and motor areas, in addition to increased ALFF of the precuneus and inferior temporal gyrus (Wu et al., 2016). The results of the current study in early adulthood support this research by demonstrating a persistence of reduced ALFF in bilateral superior temporal gyri. The findings also cohere with task-based and resting-state functional imaging research demonstrating specific functional deficits associated with temporal gyri (Bauml et al., 2014; Gozzo et al., 2009; Schafer et al., 2009; White et al., 2014; Wilke, Hauser, Krageloh-Mann, & Lidzba, 2014). Combined, the results suggest that superior temporal functional deficits that are present in infancy persist into early adulthood and are a stable pathophysiological marker of preterm birth. Further research using longitudinal designs is required to investigate this hypothesis.

Thalamic ALFF increases were also found, which were partially overlapping with the thalamic decreases in volume. These findings agree with previous univariate region-of-interest network-based analyses using largely the same patient cohort (Bauml et al., 2014) demonstrating increased functional connectivity between this region and others. When combined with the previously described research demonstrating early thalamic lesions with later MRI volume changes, the results suggest that increased ALFF may be a downstream functional correlate in young adulthood of early thalamic damage. Interestingly, a previous study investigating ALFF in infants rather than adults did not find thalamic abnormalities (Wu et al., 2016), which may suggest early functional compensation that does not persist into adulthood or secondary disruption to development of functional networks (Fair et al., 2009).

In addition to increased ALFF in thalamus, more widespread increases were found in the pre- and post-central gyri. These results are similar to previous preterm studies that have found disrupted functional connectivity of sensorimotor networks in premature neonates (Linke et al., 2018) and in perceptual and motor networks more broadly in adults born preterm, including the sensorimotor, visual, and auditory networks (Bauml et al., 2014). Similar primary damage and secondary disease effects may explain these results. In particular, cortico-striatal-thalamic pathways connect sensorimotor areas (Leisman, Braun-Benjamin, & Melillo, 2014;

TABLE 4 Correlation between decision scores for VPT/VLBW group based on GMV and ALFF, respectively, and clinical-performance scores

	GMV		ALFF	
Clinical-performance variables	ρ	p	ρ	p
Maternal age	0.098	.349	0.148	.155
Gestational age	0.343	**.008**[a]	0.283	**.030**[a]
Birth weight	0.461	**<.001**[a]	0.346	**.009**[a]
Hospital days	−0.455	**<.001**[a]	−0.354	**.005**[a]
Intensity of neonatal treatment (morbidity) index	−0.289	**.035**[a]	−0.195	.236
Duration of neonatal treatment (morbidity) index	−0.408	**<.001**[a]	−0.348	**.008**[a]
Optimality score of neonatal conditions	−0.263	.06	−0.171	.3
Performance IQ	0.140	.561	0.352	**.007**[a]
Verbal IQ	0.158	.685	0.161	.26
Full scale IQ	0.145	.684	0.303	**.024**[a]
TIV	−0.115	.542	--	--

Note: Spearman correlation between decision scores for VPT/VLBW group based on amplitude of low frequency fluctuations (ALFF) and gray matter volume (GMV). The result of p value was corrected by Holm-Bonferroni correction.
Abbreviations: IQ, intelligence quotient; ρ Spearman's rho; TIV total intracranial volume.
[a]Correlation is significant at the 0.05 level.

Marsden, 1987; Nambu, 2004) and the suspected structural damage to the subcortical areas as found in this study could result in disrupted connectivity and subsequently increased amplitude of low frequency fluctuations. This hypothesis is supported by diffusion tensor findings indicating disruption to basal ganglia and to motor connections (Hüppi et al., 1998) and by research indicating impairments in thalamocortical development related to sensory activation from 29 to 32 weeks in preterm infants (Kostovic & Judas, 2010).

4.3 | Distinction and intersection of GMV and ALFF patterns

Except for areas in the temporal lobes and thalamus, the regions discussed above largely did not overlap for each modality. Such dissociation has been reported previously in infants and adults (Baldoli et al., 2015; Salvan et al., 2014) and could represent dissociations of structural and functional development coupled with compensatory effects. On one hand, nonoverlapping increased ALFF of the sensorimotor cortices found across studies is primary thalamic and subcortical damage with subsequent functional disruption to areas whose structural development has returned to normal in adulthood. On the other hand, increased volume of the frontal, medial frontal, and posterior cingulate cortex could be due to delayed synaptic pruning in combination with functional compensation or delayed functional impairment.

In contrast, the temporal lobes were important to the classification of adults born prematurely in both the GMV and ALFF data but the direction of the results diverged. First, extensively *decreased* brain volume in the middle temporal gyri was found and this was related to *increased* ALFF. This finding is intriguing because the direction of the effect corresponds to the suspected thalamic damage, as indicated by volume reductions, which was coupled with ALFF increases as discussed earlier. The pathology underlying these findings is potentially related to abnormal growth of subplate neurons in the lateral temporal regions, which is known to be disrupted during premature birth (W. Deng, 2010; Kinney et al., 2012; Salmaso, Jablonska, Scafidi, Vaccarino, & Gallo, 2014; Joseph J. Volpe, 2009). As such, the results may suggest that primary subcortical and cortical abnormalities are related to increased ALFF—that is, as primary functional marker of brain pathology.

Second, *increased* superior temporal gyri volume was found in adults born prematurely but was related to *decreased* ALFF. As discussed earlier, the finding of increased volume is hypothesized to be related to secondary pathological cascades affecting cortical pruning as mediated by white matter tracts. However, the increased volume of other regions (e.g., medial and frontal regions) was not associated with ALFF changes in this study, which suggests a potential dissociation of the mechanism. Because superior temporal gyri abnormalities of brain functioning are so frequently reported from infancy to adulthood, these findings may suggest that persistent functional disruptions occurring throughout the lifetime may also impair neurodevelopmental processes—that is, this speculative hypothesis implies that there may be primary functional changes that then result in secondary volume changes. However, further longitudinal research is required to tease apart the dynamics of structural and functional changes.

4.4 | Clinical and cognitive relationships with brain signatures

The brain signatures of both the GMV and ALFF modalities were validated by strong relationships between an individual's decision score and preterm birth complications that are known to be associated with early brain pathology (i.e., more hospital days and lower birth weight) (Volpe, 2009). These results suggest a continuum between the severity of preterm birth complications and later brain differences when compared to individuals born full-term. Additionally, the clinical signature associated with ALFF also included performance IQ, which provides discriminant validity and highlights the importance of assessing brain functioning in order to detect similarly dynamic cognitive processes. Our further analyses also demonstrated that the prediction of general IQ was improved by the addition of the ALFF decision score. This result highlights a promising future direction for functional MRI predictive analyses because it tentatively suggests that improvements in accuracy may allow the techniques to be used as a proxy for traditional cognitive batteries in combination with birth-related variables (Dubois et al., 2018). Specifically, high prediction error was noted in the high (>110) and low (<90) IQ ranges, thus further research is needed using larger samples to improve predictive capacity (see Data S1).

In further research, it would also be beneficial to investigate departures from the relationships found in this study (e.g., individuals with high birth complications but low brain correspondence with

preterm birth signatures) in order to identify potential vulnerability and resilience factors that influence long-term brain outcomes. A hypothesis generated from this study would be that these factors would particularly modify downstream neurodevelopment, as represented by the cortical components of the brain signatures found here.

4.5 | Strength and limitations

This study was limited by a number of factors. The first is that the sample used had less morbidity than previous samples in the literature in terms of neonatal complications, functional impairments, and decreased intelligence (e.g., individuals with frank brain damage were excluded from the study). As such, the hypotheses related to primary neuronal loss relate to the possibility of more subtle brain damage that would require more direct measurement in infancy in future studies. Second, hypotheses related to neurodevelopmental disruption were based on a single, cross-sectional snapshot and longitudinal studies across the lifespan are required to fully investigate the possibility of neurodevelopmental disruption. Third, head motion during scanning and across centers may have confounded ALFF measurements despite the efforts to control for such factors. Fourth, classification error was significantly higher in the VP/VLBW group than in the FT group, which may be related to increased heterogeneity of long-term outcomes due to vulnerability and resilience factors, but this requires further investigation. In order to address these limitations, future studies should attempt to directly measure brain damage following preterm birth, follow individuals through critical developmental windows leading to adulthood, and assess vulnerability and resilience factors along this trajectory.

5 | CONCLUSION

Using multivariate machine learning techniques, this study suggests that volumetric imaging related to subcortical brain damage present in infancy also appears in early adulthood. These abnormalities are interconnected with cortical brain patterns that suggest secondary neurodevelopmental disruption persisting into adulthood. Distinctive clinical associations with each brain measure validated these young adult preterm birth signatures by reinforcing links to their birth history.

ACKNOWLEDGMENTS

We thank all current and former members of the Bavarian Longitudinal Study Group who contributed to general study organization, recruitment, and data collection, management and subsequent analyses, including (in alphabetical order): Barbara Busch, Stephan Czeschka, Claudia Grünzinger, Christian Koch, Diana Kurze, Sonja Perk, Andrea Schreier, Antje Strasser, Julia Trummer, and Eva van Rossum. We are grateful to the staff of the Department of Neuroradiology in Munich and the Department of Radiology in Bonn for their help in data collection. Most importantly, we thank all our study participants and their families for their efforts to take part in this study. This study was supported by Chinese Scholar Council (CSC, File No: 201708080036 to J.S.), Deutsche Forschungsgemeinschaft (SO 1336/1-1 to C.S.), German Federal Ministry of Education and Science (BMBF 01ER0801 to P.B. and D.W., BMBF 01ER0803 to C.S.), the Kommission für Klinische Forschung, Technische Universität München (KKF 8765162 to C.S.), and "Personalised Prognostic Tools for Early Psychosis Management" (EU-FP7 project PRONIA, Grant Agreement No. 602152 to N.K.). The authors declare no conflict of interest.

DATA AVAILABILITY STATEMENT

Participants' data used in this study are not publicly available but stored by the principle investigator of the Bavarian Longitudinal Study, and available from the corresponding author upon reasonable request.

ORCID

Jing Shang https://orcid.org/0000-0002-9816-6126

REFERENCES

Ashburner, J. (2007). A fast diffeomorphic image registration algorithm. *NeuroImage*, *38*(1), 95–113. https://doi.org/10.1016/j.neuroimage.2007.07.007

Ashburner, J., & Friston, K. J. (2005). Unified segmentation. *NeuroImage*, *26*(3), 839–851. https://doi.org/10.1016/j.neuroimage.2005.02.018

Babu, P., & Stoica, P. (2010). Spectral analysis of nonuniformly sampled data – A review. *Digital Signal Processing*, *20*(2), 359–378. https://doi.org/10.1016/j.dsp.2009.06.019

Baldoli, C., Scola, E., Della Rosa, P. A., Pontesilli, S., Longaretti, R., Poloniato, A., … Scifo, P. (2015). Maturation of preterm newborn brains: A fMRI-DTI study of auditory processing of linguistic stimuli and white matter development. *Brain Structure & Function*, *220*(6), 3733–3751. https://doi.org/10.1007/s00429-014-0887-5

Ball, G., Boardman, J. P., Rueckert, D., Aljabar, P., Arichi, T., Merchant, N., … Counsell, S. J. (2012). The effect of preterm birth on thalamic and cortical development. *Cerebral Cortex*, *22*(5), 1016–1024. https://doi.org/10.1093/cercor/bhr176

Bauml, J. G., Daamen, M., Meng, C., Neitzel, J., Scheef, L., Jaekel, J., … Sorg, C. (2014). Correspondence between aberrant intrinsic network connectivity and gray-matter volume in the ventral brain of preterm born adults. *Cerebral Cortex*, *25*, 4135–4145. https://doi.org/10.1093/cercor/bhu133

Biswal, B. B., Mennes, M., Zuo, X. N., Gohel, S., Kelly, C., Smith, S. M., … Milham, M. P. (2010). Toward discovery science of human brain function. *Proceedings of the National Academy of Sciences of the United States of America*, *107*(10), 4734–4739. https://doi.org/10.1073/pnas.0911855107

Bjuland, K. J., Rimol, L. M., Lohaugen, G. C., & Skranes, J. (2014). Brain volumes and cognitive function in very-low-birth-weight (VLBW) young adults. *European Journal of Paediatric Neurology*, *18*(5), 578–590. https://doi.org/10.1016/j.ejpn.2014.04.004

Boardman, J. P., Counsell, S. J., Rueckert, D., Kapellou, O., Bhatia, K. K., Aljabar, P., … Edwards, A. D. (2006). Abnormal deep grey matter development following preterm birth detected using deformation-based morphometry. *NeuroImage*, *32*(1), 70–78. https://doi.org/10.1016/j.neuroimage.2006.03.029

Breeman, L. D., Jaekel, J., Baumann, N., Bartmann, P., & Wolke, D. (2015). Preterm cognitive function into adulthood. *Pediatrics*, *136*(3), 415–423. https://doi.org/10.1542/peds.2015-0608

Chao-Gan, Y., & Yu-Feng, Z. (2010). DPARSF: A MATLAB toolbox for "pipeline" data analysis of resting-state fMRI. *Frontiers in Systems Neuroscience*, *4*, 13. https://doi.org/10.3389/fnsys.2010.00013

Counsell, S. J., Dyet, L. E., Larkman, D. J., Nunes, R. G., Boardman, J. P., Allsop, J. M., … Edwards, A. D. (2007). Thalamo-cortical connectivity in children born preterm mapped using probabilistic magnetic resonance tractography. *NeuroImage*, *34*(3), 896–904. https://doi.org/10.1016/j.neuroimage.2006.09.036

Cui, J., Tymofiyeva, O., Desikan, R., Flynn, T., Kim, H., Gano, D., … Xu, D. (2017). Microstructure of the default mode network in preterm infants. *AJNR. American Journal of Neuroradiology*, *38*(2), 343–348. https://doi.org/10.3174/ajnr.A4997

Cunningham, S. I., Tomasi, D., & Volkow, N. D. (2017). Structural and functional connectivity of the precuneus and thalamus to the default mode network. *Human Brain Mapping*, *38*(2), 938–956. https://doi.org/10.1002/hbm.23429

Daamen, M., Bauml, J. G., Scheef, L., Meng, C., Jurcoane, A., Jaekel, J., … Boecker, H. (2015). Neural correlates of executive attention in adults born very preterm. *Neuroimage Clin*, *9*, 581–591. https://doi.org/10.1016/j.nicl.2015.09.002

Daamen, M., Bauml, J. G., Scheef, L., Sorg, C., Busch, B., Baumann, N., … Boecker, H. (2014). Working memory in preterm-born adults: Load-dependent compensatory activity of the posterior default mode network. *Human Brain Mapping*, *36*, 1121–1137. https://doi.org/10.1002/hbm.22691

de Kieviet, J. F., Zoetebier, L., van Elburg, R. M., Vermeulen, R. J., & Oosterlaan, J. (2012). Brain development of very preterm and very low-birthweight children in childhood and adolescence: A meta-analysis. *Developmental Medicine and Child Neurology*, *54*(4), 313–323. https://doi.org/10.1111/j.1469-8749.2011.04216.x

de Vries, L. S., Benders, M. J., & Groenendaal, F. (2015). Progress in neonatal neurology with a focus on neuroimaging in the preterm infant. *Neuropediatrics*, *46*(4), 234–241. https://doi.org/10.1055/s-0035-1554102

Degnan, A. J., Wisnowski, J. L., Choi, S., Ceschin, R., Bhushan, C., Leahy, R. M., … Panigrahy, A. (2015). Altered structural and functional connectivity in late preterm preadolescence: An anatomic seed-based study of resting state networks related to the posteromedial and lateral parietal cortex. *PLoS One*, *10*(6), e0130686. https://doi.org/10.1371/journal.pone.0130686

Deng, W. (2010). Neurobiology of injury to the developing brain. *Nature Reviews. Neurology*, *6*(6), 328–336. https://doi.org/10.1038/nrneurol.2010.53

Deng, Z., Chandrasekaran, B., Wang, S., & Wong, P. C. (2016). Resting-state low-frequency fluctuations reflect individual differences in spoken language learning. *Cortex*, *76*, 63–78. https://doi.org/10.1016/j.cortex.2015.11.020

Dubois, J., Galdi, P., Paul, L. K., & Adolphs, R. (2018). A distributed brain network predicts general intelligence from resting-state human neuroimaging data. *Philosophical Transactions of the Royal Society of London. Series B, Biological Sciences*, *373*(1756), 20170284. https://doi.org/10.1098/rstb.2017.0284

Dubowitz, L. M., Dubowitz, V., & Goldberg, C. (1970). Clinical assessment of gestational age in the newborn infant. *The Journal of Pediatrics*, *77*(1), 1–10.

Fair, D. A., Cohen, A. L., Dosenbach, N. U., Church, J. A., Miezin, F. M., Barch, D. M., … Schlaggar, B. L. (2008). The maturing architecture of the brain's default network. *Proceedings of the National Academy of Sciences of the United States of America*, *105*(10), 4028–4032. https://doi.org/10.1073/pnas.0800376105

Fair, D. A., Cohen, A. L., Power, J. D., Dosenbach, N. U., Church, J. A., Miezin, F. M., … Petersen, S. E. (2009). Functional brain networks develop from a "local to distributed" organization. *PLoS Computational Biology*, *5*(5), e1000381. https://doi.org/10.1371/journal.pcbi.1000381

Froudist-Walsh, S., Karolis, V., Caldinelli, C., Brittain, P. J., Kroll, J., Rodriguez-Toscano, E., … Nosarti, C. (2015). Very early brain damage leads to remodeling of the working memory system in adulthood: A combined fMRI/-Tractography study. *The Journal of Neuroscience*, *35*(48), 15787–15799. https://doi.org/10.1523/JNEUROSCI.4769-14.2015

Gozzo, Y., Vohr, B., Lacadie, C., Hampson, M., Katz, K. H., Maller-Kesselman, J., … Ment, L. R. (2009). Alterations in neural connectivity in preterm children at school age. *NeuroImage*, *48*(2), 458–463. https://doi.org/10.1016/j.neuroimage.2009.06.046

Grothe, M. J., Scheef, L., Bauml, J., Meng, C., Daamen, M., Baumann, N., … Sorg, C. (2017). Reduced cholinergic basal forebrain integrity links neonatal complications and adult cognitive deficits after premature birth. *Biological Psychiatry*, *82*(2), 119–126. https://doi.org/10.1016/j.biopsych.2016.12.008

Gutbrod, T., Wolke, D., Soehne, B., Ohrt, B., & Riegel, K. (2000). Effects of gestation and birth weight on the growth and development of very low birthweight small for gestational age infants: A matched group comparison. *Archives of Disease in Childhood - Fetal and Neonatal Edition*, *82*(3), F208–F214.

Hare, S. M., Ford, J. M., Ahmadi, A., Damaraju, E., Belger, A., Bustillo, J., … Functional Imaging Biomedical Informatics Research, N. (2016). Modality-dependent impact of hallucinations on low-frequency fluctuations in schizophrenia. *Schizophrenia Bulletin*, *43*(2), 389–396. https://doi.org/10.1093/schbul/sbw093

Haynes, R. L., Sleeper, L. A., Volpe, J. J., & Kinney, H. C. (2013). Neuropathologic studies of the encephalopathy of prematurity in the late preterm infant. *Clinics in Perinatology*, *40*(4), 707–722. https://doi.org/10.1016/j.clp.2013.07.003

Hoerder-Suabedissen, A., & Molnar, Z. (2015). Development, evolution and pathology of neocortical subplate neurons. *Nature Reviews. Neuroscience*, *16*(3), 133–146. https://doi.org/10.1038/nrn3915

Hüppi, P. S., Maier, S. E., Peled, S., Zientara, G. P., Barnes, P. D., Jolesz, F. A., & Volpe, J. J. (1998). Microstructural development of human newborn cerebral White matter assessed in vivo by diffusion tensor magnetic resonance imaging. *Pediatric Research*, *44*, 584–590. https://doi.org/10.1203/00006450-199810000-00019

Itahashi, T., Yamada, T., Watanabe, H., Nakamura, M., Ohta, H., Kanai, C., … Hashimoto, R. (2015). Alterations of local spontaneous brain activity and connectivity in adults with high-functioning autism spectrum disorder. *Mol Autism*, *6*, 30. https://doi.org/10.1186/s13229-015-0026-z

Jonsson, P., & Wohlin, C. (2004). *An evaluation of k-nearest neighbour imputation using likert data*. Software Metrics, 2004. Proceedings. 10th International Symposium on. IEEE.

Jurcoane, A., Daamen, M., Scheef, L., J, G. B., Meng, C., A, M. W., … Boecker, H. (2015). White matter alterations of the corticospinal tract in adults born very preterm and/or with very low birth weight. *Human Brain Mapping*, *37*, 289–299. https://doi.org/10.1002/hbm.23031

Karolis, V. R., Froudist-Walsh, S., Kroll, J., Brittain, P. J., Tseng, C.-E. J., Nam, K.-W., … Nosarti, C. (2017). Volumetric grey matter alterations in adolescents and adults born very preterm suggest accelerated brain maturation. *NeuroImage*, *163*, 379–389. https://doi.org/10.1016/j.neuroimage.2017.09.039

Kinney, H. C., Haynes, R. L., Xu, G., Andiman, S. E., Folkerth, R. D., Sleeper, L. A., & Volpe, J. J. (2012). Neuron deficit in the white matter and subplate in periventricular leukomalacia. *Annals of Neurology*, *71*(3), 397–406. https://doi.org/10.1002/ana.22612

Kostovic, I., & Judas, M. (2010). The development of the subplate and thalamocortical connections in the human foetal brain. *Acta Paediatrica*, *99*(8), 1119–1127. https://doi.org/10.1111/j.1651-2227.2010.01811.x

Koutsouleris, N., Meisenzahl, E. M., Borgwardt, S., Riecher-Rossler, A., Frodl, T., Kambeitz, J., … Davatzikos, C. (2015). Individualized differential diagnosis of schizophrenia and mood disorders using

neuroanatomical biomarkers. *Brain*, *138*(Pt 7, 2059–2073. https://doi.org/10.1093/brain/awv111

Lax, I. D., Duerden, E. G., Lin, S. Y., Mallar Chakravarty, M., Donner, E. J., Lerch, J. P., & Taylor, M. J. (2013). Neuroanatomical consequences of very preterm birth in middle childhood. *Brain Structure & Function*, *218* (2), 575–585. https://doi.org/10.1007/s00429-012-0417-2

Lean, R. E., Melzer, T. R., Bora, S., Watts, R., & Woodward, L. J. (2017). Attention and regional gray matter development in very preterm children at age 12 years. *Journal of the International Neuropsychological Society*, *23*(7), 539–550. https://doi.org/10.1017/S1355617717000388

Leisman, G., Braun-Benjamin, O., & Melillo, R. (2014). Cognitive-motor interactions of the basal ganglia in development. *Frontiers in Systems Neuroscience*, *8*, 16. https://doi.org/10.3389/fnsys.2014.00016

Li, F., He, N., Li, Y., Chen, L., Huang, X., Lui, S., … Gong, Q. (2014). Intrinsic brain abnormalities in attention deficit hyperactivity disorder: A resting-state functional MR imaging study. *Radiology*, *272*(2), 514–523. https://doi.org/10.1148/radiol.14131622

Li, R., Li, Y., An, D., Gong, Q., Zhou, D., & Chen, H. (2015). Altered regional activity and inter-regional functional connectivity in psychogenic non-epileptic seizures. *Scientific Reports*, *5*, 11635. https://doi.org/10.1038/srep11635

Linke, A. C., Wild, C., Zubiaurre-Elorza, L., Herzmann, C., Duffy, H., Han, V. K., … Cusack, R. (2018). Disruption to functional networks in neonates with perinatal brain injury predicts motor skills at 8months. *Neuroimage Clin*, *18*, 399–406. https://doi.org/10.1016/j.nicl.2018.02.002

Loh, W. Y., Anderson, P. J., Cheong, J. L. Y., Spittle, A. J., Chen, J., Lee, K. J., … Thompson, D. K. (2017). Neonatal basal ganglia and thalamic volumes: Very preterm birth and 7-year neurodevelopmental outcomes. *Pediatric Research*, *82*(6), 970–978. https://doi.org/10.1038/pr.2017.161

Lui, S., Yao, L., Xiao, Y., Keedy, S. K., Reilly, J. L., Keefe, R. S., … Sweeney, J. A. (2015). Resting-state brain function in schizophrenia and psychotic bipolar probands and their first-degree relatives. *Psychological Medicine*, *45*(1), 97–108. https://doi.org/10.1017/S003329171400110X

Marsden, C. D. (1987). What do the basal ganglia tell premotor cortical areas? *Ciba Foundation Symposium*, *132*, 282–300.

Mascali, D., DiNuzzo, M., Gili, T., Moraschi, M., Fratini, M., Maraviglia, B., … Giove, F. (2015). Intrinsic patterns of coupling between correlation and amplitude of low-frequency fMRI fluctuations are disrupted in degenerative dementia mainly due to functional disconnection. *PLoS One*, *10*(4), e0120988. https://doi.org/10.1371/journal.pone.0120988

Meda, S. A., Wang, Z., Ivleva, E. I., Poudyal, G., Keshavan, M. S., Tamminga, C. A., … Pearlson, G. D. (2015). Frequency-specific neural signatures of spontaneous low-frequency resting state fluctuations in psychosis: Evidence from bipolar-schizophrenia network on intermediate phenotypes (B-SNIP) consortium. *Schizophrenia Bulletin*, *41*(6), 1336–1348. https://doi.org/10.1093/schbul/sbv064

Meng, C., Bauml, J. G., Daamen, M., Jaekel, J., Neitzel, J., Scheef, L., … Sorg, C. (2015). Extensive and interrelated subcortical white and gray matter alterations in preterm-born adults. *Brain Structure & Function*, *221*, 2109–2121. https://doi.org/10.1007/s00429-015-1032-9

Murphy, K., Bodurka, J., & Bandettini, P. A. (2007). How long to scan? The relationship between fMRI temporal signal to noise ratio and necessary scan duration. *NeuroImage*, *34*(2), 565–574. https://doi.org/10.1016/j.neuroimage.2006.09.032

Nambu, A. (2004). A new dynamic model of the cortico-basal ganglia loop, *143*, 461–466. https://doi.org/10.1016/s0079-6123(03)43043-4

Nosarti, C., Giouroukou, E., Healy, E., Rifkin, L., Walshe, M., Reichenberg, A., … Murray, R. M. (2008). Grey and white matter distribution in very preterm adolescents mediates neurodevelopmental outcome. *Brain*, *131*(Pt 1), 205–217. https://doi.org/10.1093/brain/awm282

Nosarti, C., Mechelli, A., Herrera, A., Walshe, M., Shergill, S. S., Murray, R. M., … Allin, M. P. (2011). Structural covariance in the cortex of very preterm adolescents: A voxel-based morphometry study. *Human Brain Mapping*, *32*(10), 1615–1625. https://doi.org/10.1002/hbm.21133

Nosarti, C., Nam, K. W., Walshe, M., Murray, R. M., Cuddy, M., Rifkin, L., & Allin, M. P. (2014). Preterm birth and structural brain alterations in early adulthood. *Neuroimage Clin*, *6*, 180–191. https://doi.org/10.1016/j.nicl.2014.08.005

Peterson, B. S., Vohr, B., Staib, L. H., Cannistraci, C. J., Dolberg, A., Schneider, K. C., … Ment, L. R. (2000). REgional brain volume abnormalities and long-term cognitive outcome in preterm infants. *Jama*, *284*(15), 1939–1947. https://doi.org/10.1001/jama.284.15.1939

Power, J. D., Barnes, K. A., Snyder, A. Z., Schlaggar, B. L., & Petersen, S. E. (2012). Spurious but systematic correlations in functional connectivity MRI networks arise from subject motion. *NeuroImage*, *59*(3), 2142–2154. https://doi.org/10.1016/j.neuroimage.2011.10.018

Riegel, K., Orth, B., Wolke, D., & Osterlund, K. (1995). The resting brain: Unconstrained yet reliable. In *Die Entwicklung gefährdet geborener Kinder bis zum 5 Lebensjahr*. Stuttgart, Germany: Thieme. https://doi.org/10.1093/cercor/bhn256

Salmaso, N., Jablonska, B., Scafidi, J., Vaccarino, F. M., & Gallo, V. (2014). Neurobiology of premature brain injury. *Nature Neuroscience*, *17*(3), 341–346. https://doi.org/10.1038/nn.3604

Salvan, P., Froudist Walsh, S., Allin, M. P., Walshe, M., Murray, R. M., Bhattacharyya, S., … Nosarti, C. (2014). Road work on memory lane--functional and structural alterations to the learning and memory circuit in adults born very preterm. *NeuroImage*, *102*(Pt 1), 152–161. https://doi.org/10.1016/j.neuroimage.2013.12.031

Sanchez-Vives, M. V., Massimini, M., & Mattia, M. (2017). Shaping the default activity pattern of the cortical network. *Neuron*, *94*(5), 993–1001. https://doi.org/10.1016/j.neuron.2017.05.015

Schafer, R. J., Lacadie, C., Vohr, B., Kesler, S. R., Katz, K. H., Schneider, K. C., … Ment, L. R. (2009). Alterations in functional connectivity for language in prematurely born adolescents. *Brain*, *132*(Pt 3, 661–670. https://doi.org/10.1093/brain/awn353

Scheinost, D., Kwon, S. H., Lacadie, C., Vohr, B. R., Schneider, K. C., Papademetris, X., … Ment, L. R. (2015). Alterations in anatomical covariance in the prematurely born. *Cerebral Cortex*, *27*(1), 534–543. https://doi.org/10.1093/cercor/bhv248

Shang, J., Bauml, J. G., Koutsouleris, N., Daamen, M., Baumann, N., Zimmer, C., … Sorg, C. (2018). Decreased BOLD fluctuations in lateral temporal cortices of premature born adults. *Human Brain Mapping*, *39*, 4903–4912. https://doi.org/10.1002/hbm.24332

Smyser, C. D., Snyder, A. Z., Shimony, J. S., Blazey, T. M., Inder, T. E., & Neil, J. J. (2013). Effects of white matter injury on resting state fMRI measures in prematurely born infants.

Sowell, E. R., Thompson, P. M., Holmes, C. J., Jernigan, T. L., & Toga, A. W. (1999). In vivo evidence for post-adolescent brain maturation in frontal and striatal regions. *Nature Neuroscience*, *2*(10), 859–861. https://doi.org/10.1038/13154

Takeuchi, H., Taki, Y., Nouchi, R., Sekiguchi, A., Hashizume, H., Sassa, Y., … Kawashima, R. (2015). Degree centrality and fractional amplitude of low-frequency oscillations associated with Stroop interference. *NeuroImage*, *119*, 197–209. https://doi.org/10.1016/j.neuroimage.2015.06.058

Thompson, D. K., Lee, K. J., Egan, G. F., Warfield, S. K., Doyle, L. W., Anderson, P. J., & Inder, T. E. (2014). Regional white matter microstructure in very preterm infants: Predictors and 7 year outcomes. *Cortex*, *52*, 60–74. https://doi.org/10.1016/j.cortex.2013.11.010

Tsimis, M. E., Johnson, C. T., Raghunathan, R. S., Northington, F. J., Burd, I., & Graham, E. M. (2015). Risk factors for periventricular white matter injury in very low birthweight neonates. *American Journal of Obstetrics and Gynecology*, *214*, 380.e1–380.e6. https://doi.org/10.1016/j.ajog.2015.09.108

Van Dijk, K. R., Sabuncu, M. R., & Buckner, R. L. (2012). The influence of head motion on intrinsic functional connectivity MRI. *NeuroImage*, *59* (1), 431–438. https://doi.org/10.1016/j.neuroimage.2011.07.044

Volpe, J. J. (2009). Brain injury in premature infants: A complex amalgam of destructive and developmental disturbances. *The Lancet Neurology*, *8*(1), 110–124. https://doi.org/10.1016/s1474-4422(08)70294-1

Volpe, J. J. (2012). Neonatal encephalopathy: An inadequate term for hypoxic-ischemic encephalopathy. *Annals of Neurology*, *72*(2), 156–166. https://doi.org/10.1002/ana.23647

von Aster, M., Neubauer, A., & Horn, R. (2006). *Wechsler Intelligenztest für Erwachsene WIE. Deutschsprachige Bearbeitung und Adaptation des WAIS-III von David Wechsler (2., korrigierte Auflage)*. Frankfurt: Pearson Assessment.

Wan, C. Y., Wood, A. G., Chen, J., Wilson, S. J., & Reutens, D. C. (2013). The influence of preterm birth on structural alterations of the vision-deprived brain. *Cortex*, *49*(4), 1100–1109. https://doi.org/10.1016/j.cortex.2012.03.013

White, T. P., Symington, I., Castellanos, N. P., Brittain, P. J., Froudist Walsh, S., Nam, K. W., … Nosarti, C. (2014). Dysconnectivity of neurocognitive networks at rest in very-preterm born adults. *Neuroimage Clin*, *4*, 352–365. https://doi.org/10.1016/j.nicl.2014.01.005

Wilke, M., Hauser, T. K., Krageloh-Mann, I., & Lidzba, K. (2014). Specific impairment of functional connectivity between language regions in former early preterms. *Human Brain Mapping*, *35*(7), 3372–3384. https://doi.org/10.1002/hbm.22408

Wolke, D., & Meyer, R. (1999). Cognitive status, language attainment, and prereading skills of 6-year-old very preterm children and their peers: The Bavarian longitudinal study. *Developmental Medicine & Child Neurology*, *41*(02), 94–109.

Wu, X., Wei, L., Wang, N., Hu, Z., Wang, L., Ma, J., … Shi, Y. (2016). Frequency of spontaneous BOLD signal differences between moderate and late preterm newborns and term newborns. *Neurotoxicity Research*, *30*(3), 539–551. https://doi.org/10.1007/s12640-016-9642-4

Yan, C. G., Cheung, B., Kelly, C., Colcombe, S., Craddock, R. C., Di Martino, A., … Milham, M. P. (2013). A comprehensive assessment of regional variation in the impact of head micromovements on functional connectomics. *NeuroImage*, *76*, 183–201. https://doi.org/10.1016/j.neuroimage.2013.03.004

Young, J. M., Powell, T. L., Morgan, B. R., Card, D., Lee, W., Smith, M. L., … Taylor, M. J. (2015). Deep grey matter growth predicts neurodevelopmental outcomes in very preterm children. *NeuroImage*, *111*, 360–368. https://doi.org/10.1016/j.neuroimage.2015.02.030

Zang, Y. F., He, Y., Zhu, C. Z., Cao, Q. J., Sui, M. Q., Liang, M., … Wang, Y. F. (2007). Altered baseline brain activity in children with ADHD revealed by resting-state functional MRI. *Brain Dev*, *29*(2), 83–91. https://doi.org/10.1016/j.braindev.2006.07.002

Zhao, C., Zhu, J., Liu, X., Pu, C., Lai, Y., Chen, L., … Hong, N. (2017). Structural and functional brain abnormalities in schizophrenia: A cross-sectional study at different stages of the disease. *Progress in Neuro-Psychopharmacology & Biological Psychiatry*, *83*, 27–32. https://doi.org/10.1016/j.pnpbp.2017.12.017

SUPPORTING INFORMATION

Additional supporting information may be found online in the Supporting Information section at the end of this article.

How to cite this article: Shang J, Fisher P, Bäuml JG, et al. A machine learning investigation of volumetric and functional MRI abnormalities in adults born preterm. *Hum Brain Mapp*. 2019;40:4239–4252. https://doi.org/10.1002/hbm.24698